PERIODICA POLYTECHNICA SER. TRANSP. ENG. VOL. 25, NO. 1-2, PP. 59-77 (1997)

SIMULATION STUDY OF THE INFLUENCE OF INVOLUTE TIP RELIEF ON GEAR DYNAMIC BEHAVIOUR

János MÁRIALIGETI

Department of Machine Elements
Faculty of Transportation Engineering
Technical University of Budapest
H-1521 Budapest, Hungary

Received: November 13, 1996

Abstract

The tooth tip relief, as an intended departure from the normal involute profile is a common technics for the improvement of tooth contact characteristics. It is often used not only for avoiding tip contact, but especially in the case of long relief, to aim at better dynamic behaviour. For studying the dynamic characteristics of gear trains in the case of long relief, comparative computer simulations were carried out for a train with normal toothing and with tooth tip relief. The applied dynamical model and excitation characteristics are discussed. By simulating smooth acceleration processes at different nominal load conditions, resonance curves are generated and analysed in the case of ideal tooth geometry under real mesh conditions, i.e. the mesh irregularities at the beginning and points of contact, due to tooth deflections were taken into account. Dynamic behaviour at low specific load level is studied based on steady state rolling down simulations and resonance characteristics are discussed.

Keywords: gear train, tooth tip relief, gear dynamics, non-linear vibration, simulation.

1. Introduction

The vehicle transmissions in operation are subjected in general to randomly variable load conditions, characterised by considerable variations even in the load amplitude and in the frequency range. Tooth profile modifications in height direction, as the long tooth relief, see for example in [1], [2], which can improve considerably the tooth dynamic behaviour in a relatively narrow load range, are often used in vehicle transmissions, too. However, the operating load range is normally broader than the region, where the effect of the relief is optimum. Consequently, special care must be taken for the correct choice of the tip relief values and their height.

On *Fig. 1*, four successive positions of the same profile pair are shown on the pressure line for teeth with long relief. The points A and E are the beginning and end points of contact with normal profiles and $\overline{AD} = \overline{BE} = \overline{KA_{l2}} = \overline{A_{l1}M} = p_b$. Point A_{l1} is the beginning, A_{l2} is the end point of contact of the normal involute profile of gears 1 (upper) and 2, on the

diameters $d_{l1,2}$ respectively, p_b is the pitch on the base circle. The upper profile sections with thin line are the eliminated involute sections, $C_{a1,2}$ are the relief values, respectively.

Considering the pinion and wheel in positions belonging to the normal profile, there is no contact in position at point A, because of the tip relief on wheel 1, but the foregoing profile pair at point D is in normal contact. In contact position at point K, the foregoing profile pair leaves just the contact, consequently on $\overline{KA_{l1}}$, contact is only possible by rotating back gear 1. At position in point A_{l1}, the original profiles are in contact, as for the gears with normal profile and that remains up to the position in point A_{l2}. Passing A_{l2} because of the relief on gear 2, contact is possible only with rotating back gear 1, being the succeeding profile pair in the interval $\overline{KA_{l1}}$. In contact at point M, the succeeding profile pair enters in normal contact. So, on intervals $\overline{KA_{l1}}$ and $\overline{A_{l2}M}$, contact is possible only with lag of the gear behind its nominal position. In other words, the contact ratio is less than one, introducing kinematic excitation.

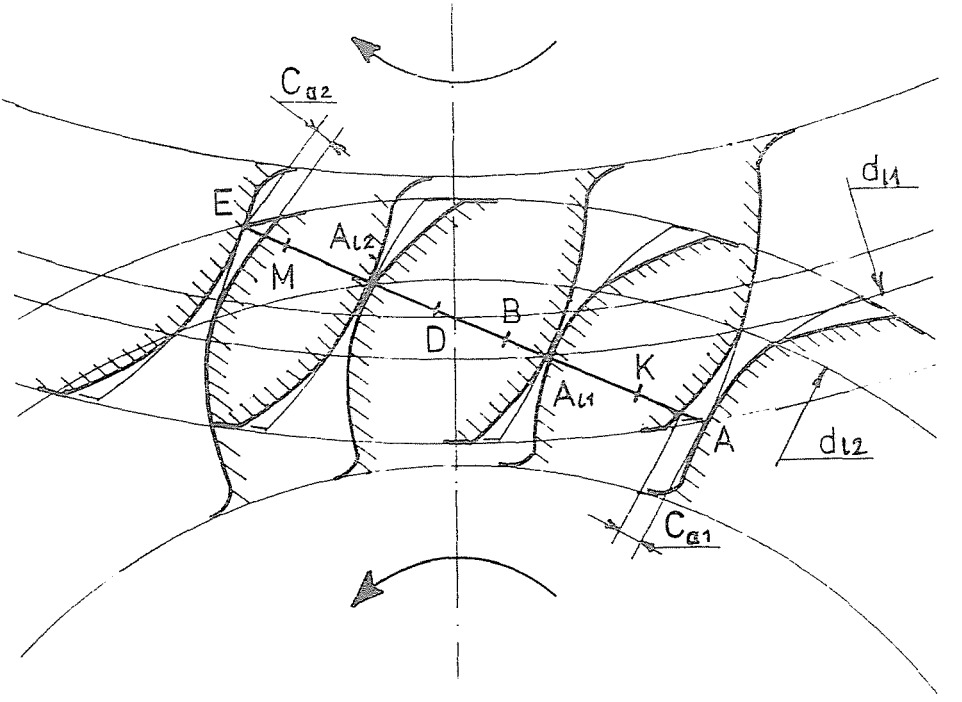

Fig. 1. Tooth contact on the pressure line for teeth with tip relief

2. The Dynamic Model

2.1. The Kinematic Excitation

For the simulation study a two mass system model is applied, with rotating masses, coupled by a spring system, as it is schematically represented on *Fig. 2.* The details of the spring system, replacing the real tooth contact, are described in detail in [3].

In the system on *Fig. 2.* the cam symbolises the resultant *kinematic excitation,* introduced by the tooth pairs, being in contact at a given contact point. The kinematic excitation is introduced by mesh irregularities due to the tooth deformations on one side, and profile relief and manufacturing errors on the other side. Consequently, for gears with ideal geometry the period of the kinematic excitation $\Omega = 2\pi/z_1$, where z_1 is the number of teeth of the pinion. For gears with manufacturing errors, Ω is the total rotation angle of the driver, rolling down during the realisation of all possible combinations of the profile pairs of the driver and the driven gear.

The description of the kinematic excitation can be conveniently handled by the *contact function,* $\delta_j(\varphi_1)$ see e.g. in [3], [4] which gives the travel error of the driven gear, measured in length on the pressure line, at any driver angular position φ_1. The subscript j refers to the jth tooth profile pair combination.

Fig. 3a shows a series of contact functions for ideal normal gears, whilst on *Fig. 3b* contact functions for profiles with tip relief are represented. The curved parts at the A and E points symbolise the errors involved by mesh irregularities at entering into and leaving the contact. Taking into consideration the contact process on the pressure line discussed in *Fig. 1* and the fact that for profiles with long relief $\varepsilon_\alpha < 1$, the $\delta(\varphi_1)$ *resultant contact function* has triangular shaped parts, where its value is not zero, see *Fig. 3b.*

2.2. Basic Dynamic Behaviour

The differential equations for the two mass system in *Fig. 2* are:

$$J_1 \cdot \ddot{\varphi}_1 + \left\{ \sum_{j=1}^{n} K_j \left(\Delta\dot{\sigma} - \dot{\delta}_j(\varphi_1) \right) \right\} r_{b1} + r_{b1} \cdot \hat{s}(\varphi_1; \Delta\sigma) \cdot \Delta\sigma = T_1,$$

$$J_2 \cdot \ddot{\varphi}_2 + \left\{ \sum_{j=1}^{n} K_j \left(\Delta\dot{\sigma} - \dot{\delta}_j(\varphi_1) \right) \right\} r_{b2} + r_{b2} \cdot \hat{s}(\varphi_1; \Delta\sigma) \cdot \Delta\sigma = -T_{21}, \quad (1)$$

where $\ddot{\varphi}_{1,2}$, $\dot{\varphi}_{1,2}$, $\varphi_{1,2}$, are the twist angles of the masses and their time derivatives, K_j is the damping coefficient in the single tooth pair contact.

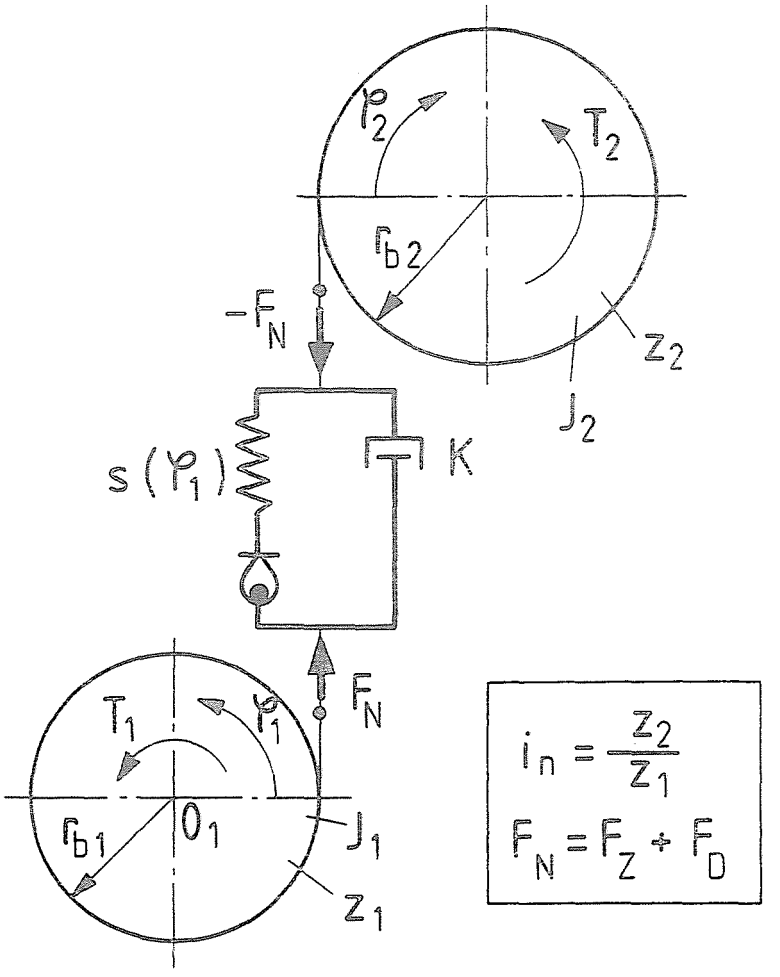

Fig. 2. Schematic two mass model. ($J_{1,2}$ moments of inertia of the rotating masses, $z_{1,2}$ number of teeth, $T_{1,2}$ outer torques, $\varphi_{1,2}$ twist angles, $r_{b1,2}$ base circle radii, $s(\varphi_1)$ tooth contact stiffness function, F_N resultant contact force on the pressure line, F_z and F_D are the elastic and damping forces in contact, K damping coefficient.)

$\Delta\sigma = w_j + \delta_j$ is the instantaneous travel error, composed from the w_j tooth deflection and δ_j contact function value for the tooth flanks actually in mesh, and $\hat{s}(\varphi_1; \Delta\sigma)$ is the *reduced stiffness function* [4]. This latter multiplied with $\Delta\sigma$ gives the actual elastic force, acting in the mesh. The

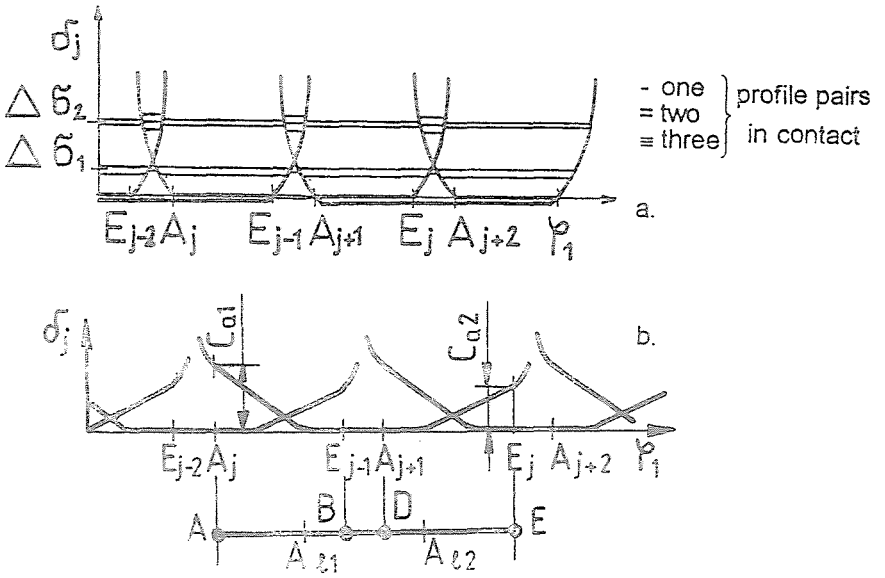

Fig. 3. Contact functions for ideal profiles (*a*) and with tip relief (*b*)

reduced stiffness function contains all excitation components, so it can be considered as the parametric excitation term in the system.

In general case, the reduced stiffness function can be written as the sum of its Fourier components C_k, with the C_0 average value as follows:

$$\hat{s}(\varphi_1;\Delta\sigma) = C_0(\Delta\sigma) + \sum_{k=1}^{\infty} C_k(\Delta\sigma)\cdot\cos\left(\frac{2\pi}{\Omega}\cdot k\varphi_1 + \nu_k\right), \qquad (2)$$

where Ω is the basic angular period of the reduced stiffness function, k is the ordering number of the Fourier components, and ν_k the phase angle.

One can distinguish the $\hat{s}(\varphi_1;\Delta\sigma)$ *stiffness function*, which is the sum of single tooth pair stiffnesses being actually in contact; consequently it differs from the reduced stiffness function. The integral mean value (average) of the stiffness function is called as gear engagement spring stiffness c_γ. In the case of linear single tooth pair stiffness characteristic (i.e. force-deflection curve at a given contact position) at each contact point and ideal tooth geometry, its value is approximately constant. However, in the case of toothing with tip relief or with manufacturing errors or/and with non-linear single tooth pair stiffness characteristic , its value is load (i.e. $\Delta\sigma$) dependent and will be marked as $\tilde{c}_\gamma$.

The system of *Eq.* (1) with the excitation term (2) describes a rheo-nonlinear type vibration [5].

The basic vibration properties of such type of vibrations for one mass system with harmonic excitation can be studied by applying the stability chart, see ex. [5].

Assuming ideal tooth geometry, without manufacturing error, the tooth frequency $f_z = z_1 \cdot n_1 = z_1 \cdot \omega_1 / 2\pi$, $\varphi_1 = \omega_1 \cdot t$, where ω_1 and n_1 are the input angular frequency and rotation speed, respectively, the period of the excitation $\Omega = 2\pi / z_1$ and the *tooth angular frequency* $\omega_z = z_1 \cdot \omega_1$, being the basic excitation angular frequency. The system eigenfrequency, $\omega_s = \sqrt{c_\gamma / m}$, see ex. [5], [2] where m is the reduced mass of the one-mass system. As it is known from the stability chart, unstable, or resonance points develop, if

$$\frac{\omega_s^2}{\omega_z^2} = \left(\frac{\nu}{2}\right)^2, \qquad \nu = 1,\ 2,\ \ldots, \infty. \tag{3}$$

Rearranging *Eq.* (3), unstable vibration develops, if the excitation frequency, $\omega_z = 2\omega_s / \nu$. *Fig. 4* shows schematically the resonance curve for such a system with damping, on the tooth angular frequency with the vibration amplitude ratio $\Delta\sigma_{max} / \Delta\sigma_{stat}$ on the vertical axis.

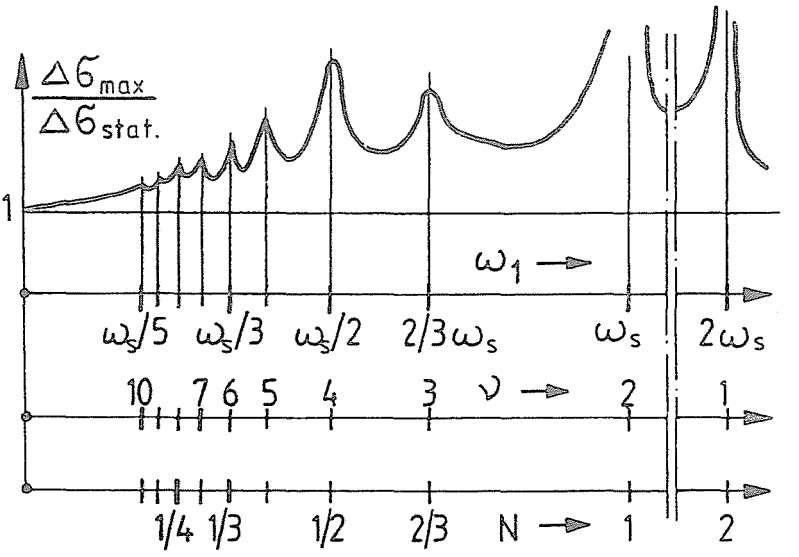

Fig. 4. Schematic resonance curve

Considering a complex excitation function with harmonic components of $k = 1,\ 2,\ \ldots, \infty$, the angular frequency of the k-th harmonic components will be $\omega_z \cdot k$. Replacing this value in *Eq.* (3) as excitation frequency, rearranging the equation and introducing $\omega_z \left(\nu^{(k)}\right)$, as the tooth frequency at which the ν-th order resonance point of the kth order harmonic excitation component develops, one can write:

$$\omega_z \left(\nu^{(k)}\right) = \frac{2\omega_s}{k \cdot \nu}, \qquad k = 1,\ 2,\ \ldots,\ \infty, \qquad \nu = 1,\ 2,\ \ldots,\ \infty. \tag{4}$$

From *Eq.* (4), the following can be concluded:

- since $k \geq 1$, $\nu \geq 1$, unstable points develop only at excitation frequencies equal to or less than $2\omega_s$,
- since k and ν are whole numbers, their product will be whole, and in turn, all whole numbers can be produced as the product of two whole numbers, consequently each whole number can serve as divisor,
- one can find unstable point at each excitation frequency which is $2\omega_s$ divided with a whole number,
- for all $\nu^{(k)} k \geq 1$, $\nu \geq 1$ with $k \cdot \nu$ =const., the resonance points are at the same excitation frequency.

However, in the presence of damping, as it is in practice, the higher order unstable points tend to lose of importance.

In the gearing technics, a dimensionless frequency ratio number N is introduced [2], for the marking of the different resonance points, as follows:

$$N = \frac{\omega_z}{\omega_s} = \frac{z_1 \cdot \omega_1}{\omega_s} = \frac{2}{\nu}, \qquad \nu = 1, 2, \ldots, \infty, \tag{5}$$

so unstable resonance points can develop at $N = 2, 1, 2/3, 1/2, \ldots$. The resonance at $N = 1$ is called as main resonance point. For cases, in which the average stiffness $\tilde{c}_\gamma$ is load dependent, the frequency ratio depends on the load, too, so in that case the symbol $\tilde{N}$ will be applied.

3. System Behaviour of Gear Trains with Normal Toothing

For studying the system behaviour, an electric locomotive main drive train is applied, with the following basic parameters: $z_1 = 53$, $z_2 = 65$, $m = 12$. The pinion and gear are constructed as hub, web and rim, which involves a decrease of the theoretical tooth stiffness, see ex. [6]. Two stiffness variants were applied, one with the theoretical stiffnesses by Weber – Banaschek [2] with linear single tooth pair stiffness function characteristic, coded as WBlin, and the other with taking into consideration the rim influence by [6] and with non-linear single tooth pair stiffness characteristic by [7], coded as WBHKp.

For characterising the system behaviour, continuous rolling down processes by smooth acceleration were simulated and the tooth contact force dynamic factor V_Σ was calculated:

$$V_\Sigma = \max_\gamma \{V_\Sigma(\varphi_1)\}; \qquad V_\Sigma(\varphi_1) = \frac{\sum_{j=1}^{n} \frac{F_{N_j}(\varphi_1)}{b}}{\frac{F_N}{b}}, \tag{6}$$

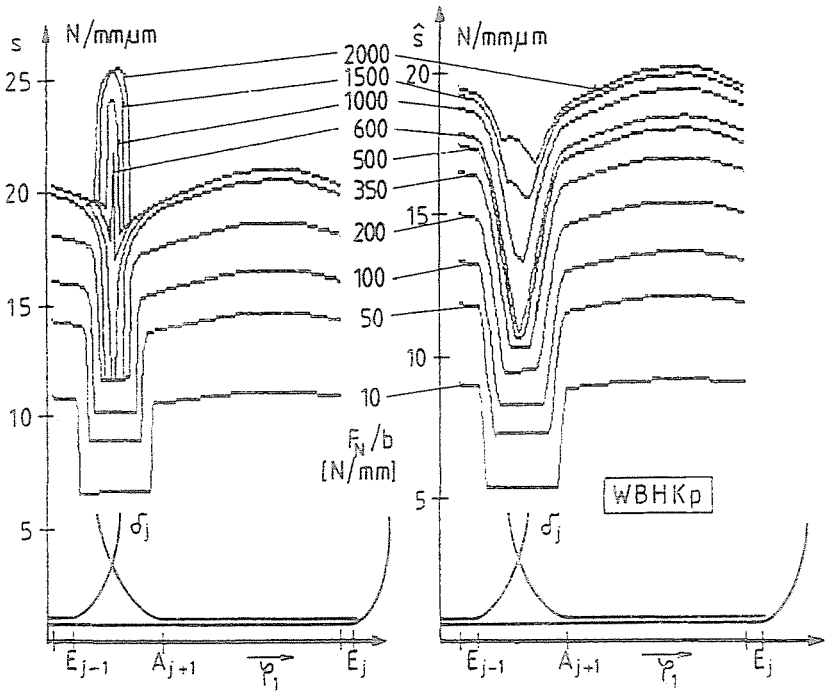

Fig. 5. Stiffness $s(\varphi_1 : \Delta\sigma)$ and reduced stiffness $\hat{s}(\varphi_1 : \Delta\sigma)$ functions for ideal, normal tooth profiles

where F_N/b is the total nominal specific load in contact, (due to the nominal outer load). F_{N_j}/b is the real, dynamical load on the jth profile pair, n being the number of teeth in contact, and γ is the rotational angle of the pinion, corresponding to one tooth mesh.

On *Fig. 5* stiffness and reduced stiffness functions are shown, with the corresponding contact functions for gear train with normal profile. Expressed load dependence is caused by the mesh irregularities and the beginning and end points of contact due to the elastic tooth deflections and by the non-linear single tooth pair stiffness characteristic [7], coded as WBHKp.

Fig. 6 represents the resonance curves for different specific load values. On *Fig. 6a*, small damping coefficient is applied with backlash h, allowing the development of the resonance points. For $N = 1$, $1/2$, $1/3$ and $1/4$ the tooth flanks separate (where $V_\Sigma = 0$), and non-linear resonance develops. That is why their location is slightly lower as it is previewed by the marked N values. On *Fig. 6b, c, d* normal damping is applied for case WBlin, resulting considerably lower load elevations in the resonance points. However, at $N = 1$ and $1/2$, and at low specific load value, tooth flank separation occurs, involving the decrease of the resonance pick location.

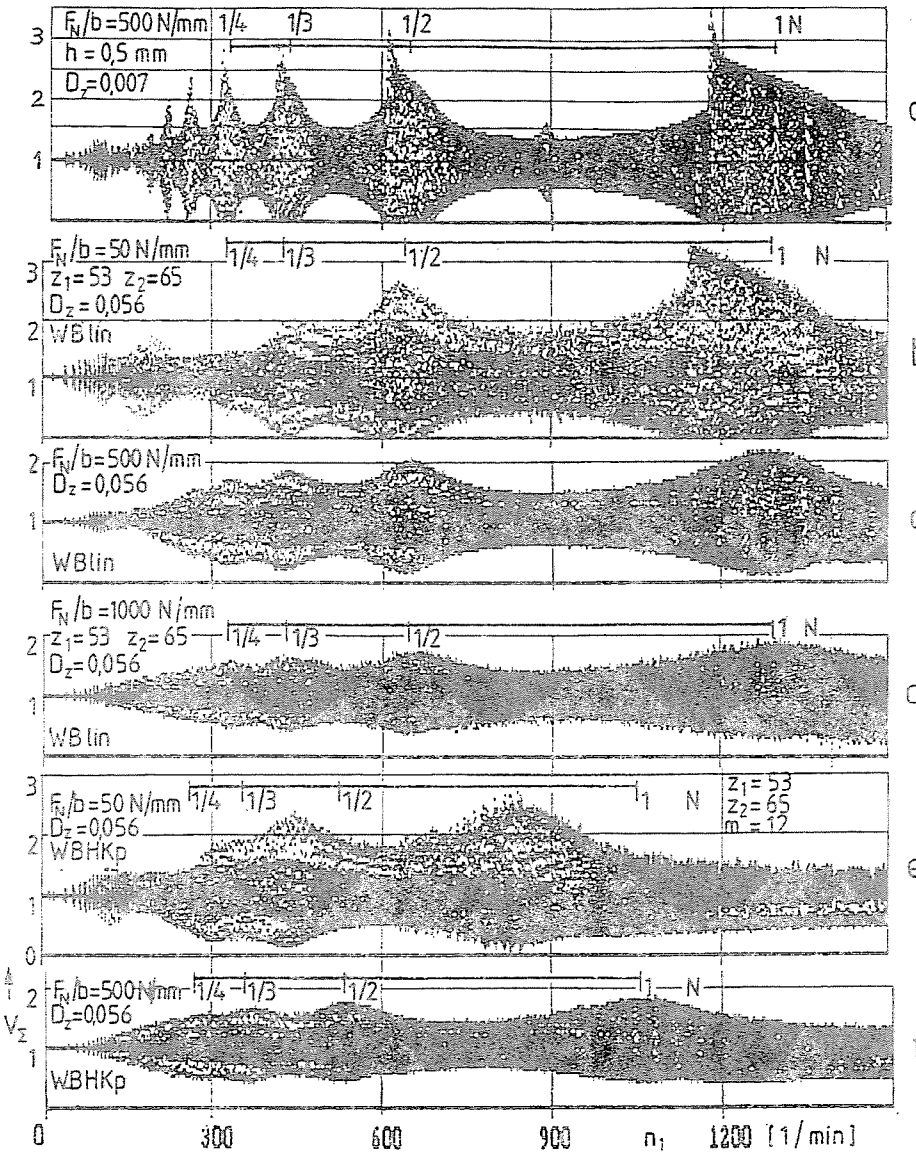

Fig. 6. Resonance curves in the case of ideal, normal tooth profiles

At higher loads regular resonance locations develop, without tooth flank separation. One can state that, at increasing load, the dynamic forces tend to decrease slightly, in agreement with experimental results. The general vibration shape changes only slightly.

On *Fig. 6e, f* the same system is represented, with lower single tooth

stiffness values and non-linear single tooth pair stiffness characteristic by *Fig. 5.* The general vibration shape remains similar, however, the resonance points move towards the lower input speeds. The reason of that is the smaller average stiffness. The difference between the theoretical N location and the real one can be explained by the fact that the beginning part of the single tooth pair stiffness function is progressive, with lower stiffnesses [7] and this is not taken into consideration in the calculation of N, determined with c_γ. Since the single tooth pair stiffness characteristics at fixed contact positions are not linear, expressed load dependence can be found on the resonance curves, see *Fig. 6e* and *f.*

Considering the curves on *Fig. 6*, in the case of linear single tooth pair stiffness characteristic, slight load dependence of the vibration shape and slight dynamic factor variation presents itself at different nominal loads, which is the result of the mesh irregularities at the points A, i.e. entering into, and E, i.e. leaving the contact of a given profile pair. For non-linear single tooth pair stiffness function, differences can be found even for vibration shape and dynamic factors.

4. System Behaviour of Gear Trains with Profile Relief

4.1. Contact Properties in the Case of Profiles with Tip Relief

In the case of tip relief, the number of tooth pairs in contact varies not only in the function of contact position, but it depends on the applied load as well. Let us consider the contact applying the contact functions, *Fig. 7.*

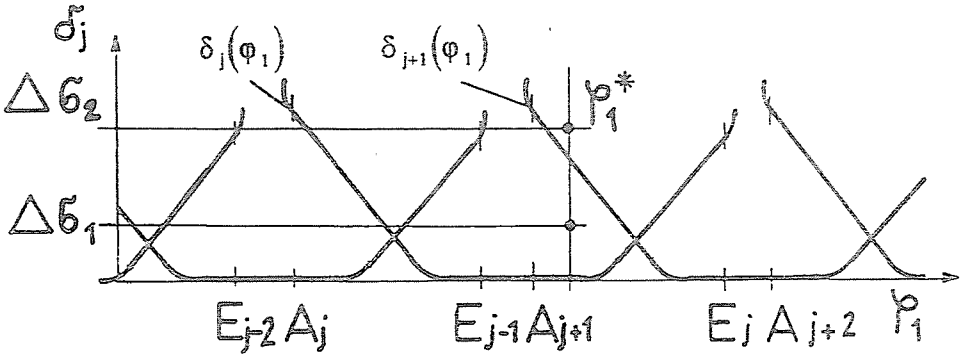

Fig. 7. Contact analysis based on contact functions

Assuming a given travel error due to a given load $\Delta\sigma_1$ =const. and $\Delta\sigma_2 > \Delta\sigma_1$, one can detect the number of teeth in contact at any position φ_1. At φ_1^* e.g. $\Delta\sigma_1 > \delta_j(\varphi_1^*)$, so the profile pair j is already in contact and profile pair $j+1$ did not enter into contact, whilst at $\Delta\sigma_2$, being

$\Delta\sigma_2 > \delta_j(\varphi_1^*)$, $\Delta\sigma_2 > \delta_{j+1}(\varphi_1^*)$, both are in contact. The contact ratio, interpreted on geometrical bases, is not applicable for the following of this phenomenon. However, introducing the real, load dependent contact ratio ε_t, by the following definition:

$$\varepsilon_t(\Delta\sigma) = \frac{1}{\Phi}\sum_{j=1}^{n}\int_{\Phi} I_j \mathrm{d}\varphi_1 \geq 1, \tag{7}$$

where Φ is an arbitrary angular interval on φ_1, and I_j is an indicator function:

$$I_j(\varphi_1;\Delta\sigma) = \begin{cases} 1 & \text{if} \quad \Delta\sigma > \delta_j(\varphi_1), \\ 0 & \text{if} \quad \Delta\sigma \leq \delta_j(\varphi_1), \end{cases} \tag{8}$$

one can calculate the average number of teeth, being in contact at any $\Delta\sigma$, i.e. at any load, F_N/b.

4.2. Excitation Properties

Since the contact conditions for profile with tip relief are load dependent, it is straightforward, that stiffness functions and reduced stiffness functions, the latter being responsible for the excitation, are load dependent, too. *Fig. 8* represents the stiffness and reduced stiffness functions, $s(\varphi_1;\Delta\sigma)$ and $\hat{s}(\varphi_1;\Delta\sigma)$, respectively, for the case of non-linear single tooth pair stiffness characteristic, WBHKp. For case of WBlin, the curve shapes are similar.

The main Fourier components $C'_k = C_k/C_0$ of the excitation functions on *Fig. 9* reflect its strong variation. (The continuous lines are applied only for the sake of the better visualisation.)

4.3. Resonance Curves

Fig. 11 represents the resonance curves for profiles with tip relief in the case of two different single tooth pair stiffness characteristics. One can detect the strong nonlinear behaviour as the nominal load varies and the important differences related to the resonance curves on *Fig. 6*, for normal profiles. The general shape of the curves is similar for both stiffness cases, however, the dynamic load values at individual operation points differ considerably.

Especially for the linear single tooth pair stiffness characteristic case, at specific load $F_N/b = 200$ N/mm and lower, the tooth flanks separate practically on the whole region. In both cases, the main resonance regions are displaced towards the lower input speed values. At small load levels, the unstable regions belonging to different N or $\tilde{N}$ values do not separate in a clear manner.

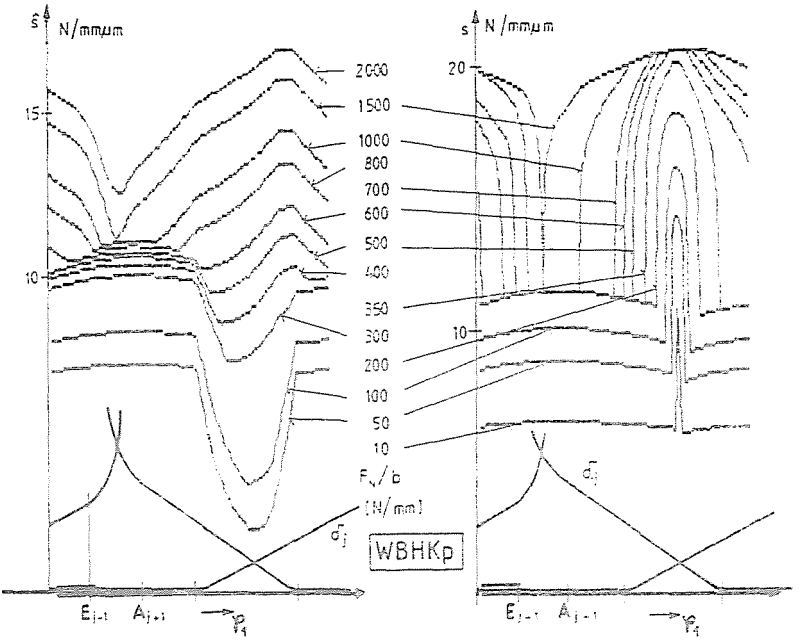

Fig. 8. Stiffness $s(\varphi_1; \Delta\sigma)$ and reduced stiffness $\tilde{s}(\varphi_1; \Delta\sigma)$ functions for ideal tooth with tip relief

Fig. 10 shows the variation of the load dependent gear engagement spring stiffness values $\tilde{c}_\gamma$, and the variation of the real contact ratio ε_γ. The $\tilde{N}$ values on *Fig. 11* are calculated with these $\tilde{c}_\gamma$ values, showing strong variations as the load varies.

On the resonance curves of WBlin, two different non-linear resonance characters can be detected. At specific load levels of $F_N/b = 50$, 100, 200 N/mm, the unstable regions are of nonlinear softening type. As namely the vibration amplitudes increase, the length of the angular intervals without contact (tooth flank separation) increase, too, consequently the average stiffness of the system which develops during the vibration decreases. In spite of that, the main resonance region at $F_N/b = 350$ N/mm, one can find a non-linear resonance of hardening type. In that case, the increasing vibration amplitudes arrive in greater stiffness regions, and fall down after. In other unstable regions normal curve shapes develop.

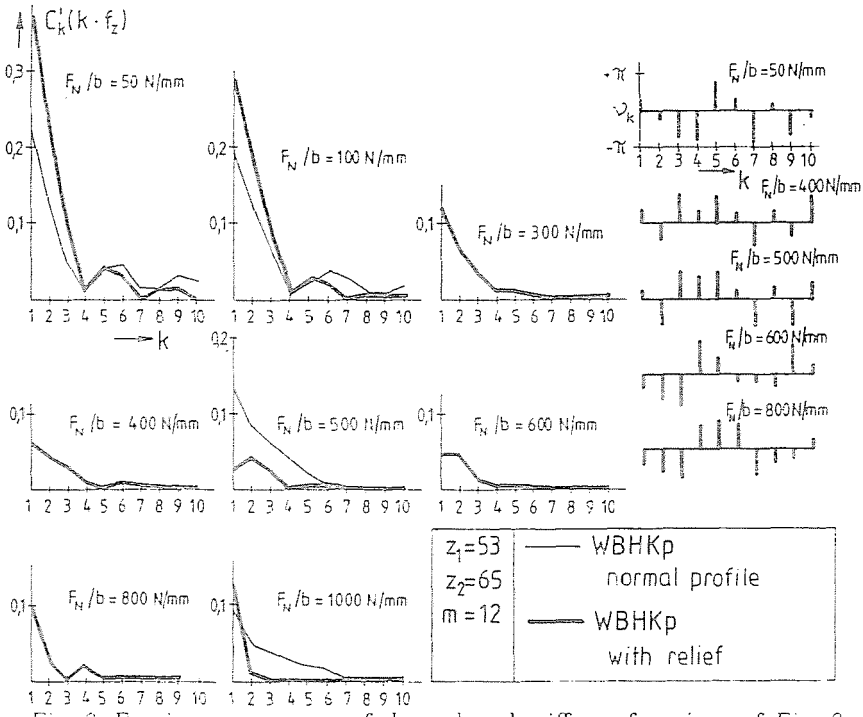

Fig. 9. Fourier components of the reduced stiffness functions of *Fig. 8*

With increasing specific loads F_N/b, the vibrations, i.e. the dynamic force elevations tend to smooth, and optimum region can be identified at about $F_N/b = 700$ N/mm for WBlin, and $F_N/b = 500$ N/mm for WBHKp. These values are in good agreement with the location of the optimum found with quasi static rolling down [4]. At higher specific loads, only the main resonance at $\tilde{N} = 1$ becomes important, on other regions the vibrations remain reduced.

Comparing this behaviour to that with normal toothing, important differences can be stated. At lower specific loads, the dynamic behaviour of gears with relief is strongly unfavourable, whilst at higher loads, optimal load interval can be found.

As consequence, one can resume that the dynamic behaviour of gears with long tooth tip relief differs considerably from that with normal one. Strong non-linear behaviour develops and optimum region can be identified. The influence of the single tooth pair stiffness characteristic has important influence on the dynamic behaviour and the location of the optimal region.

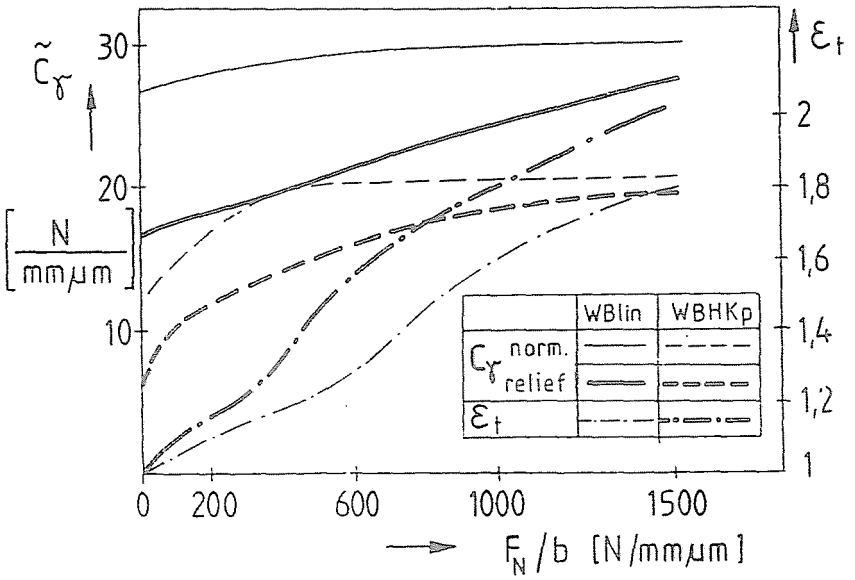

Fig. 10. Variation of real contact ratio and gear engagement stiffness in the function of the specific load

5. Analysis of the Vibrations at Lower Specific Load Values

As the resonance curves in *Fig. 11* at lower specific load levels indicate, the individual resonance regions fall together, resulting quite important dynamic factors and tooth flank separations on important input seed interval. For the more detailed analysis of these vibrations, real tooth load functions were generated, permitting the study of the contact conditions on the teeth. At some constant input speed value, continuous rolling down was simulated at load level $F_N/b = 50$ N/mm and tooth contact force dynamic factors by *Eq.* (6), and single tooth force dynamic factors $V_F(\varphi_1) = (F_{Nj}/b)/(F_N/b)$ for the individual tooth pairs were generated. On *Fig. 12* at each input speed, the upper curve is the total contact force dynamic factor variation during engagement and the curves below are the contact force dynamic factor variations for the single tooth pairs. In some cases only one tooth pair contact develops, consequently one curve is sufficient. The marking on the upper diagrams corresponds to the pitch points.

In all cases, the length of the represented angular interval φ_1 is equal to the real vibration period.

Based on the curves WBlin, the following can be concluded:

– at $n_1 = 180$/min, the period of the response vibration is the triple of

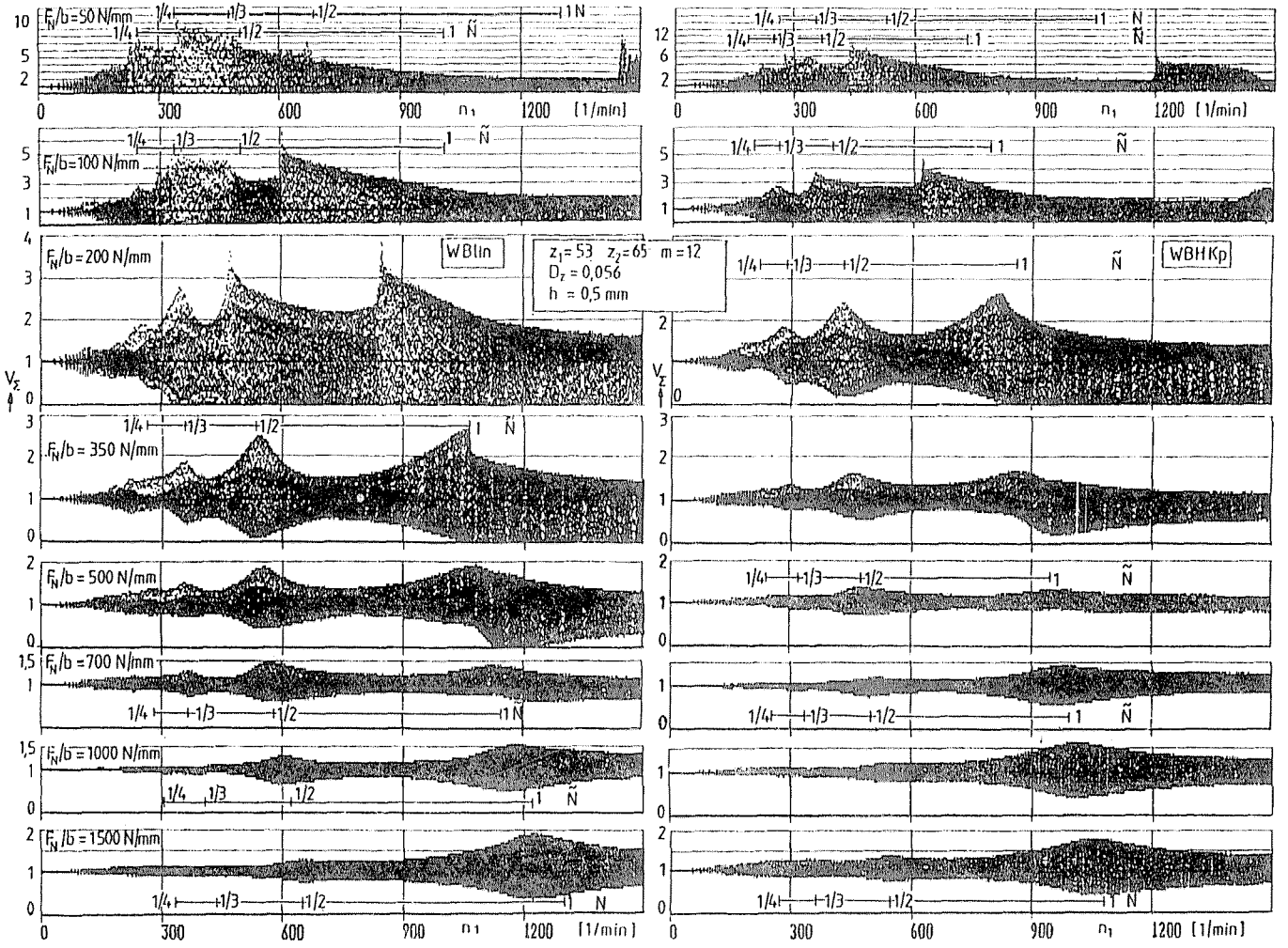

Fig. 11. Resonance curves for profiles with tip relief

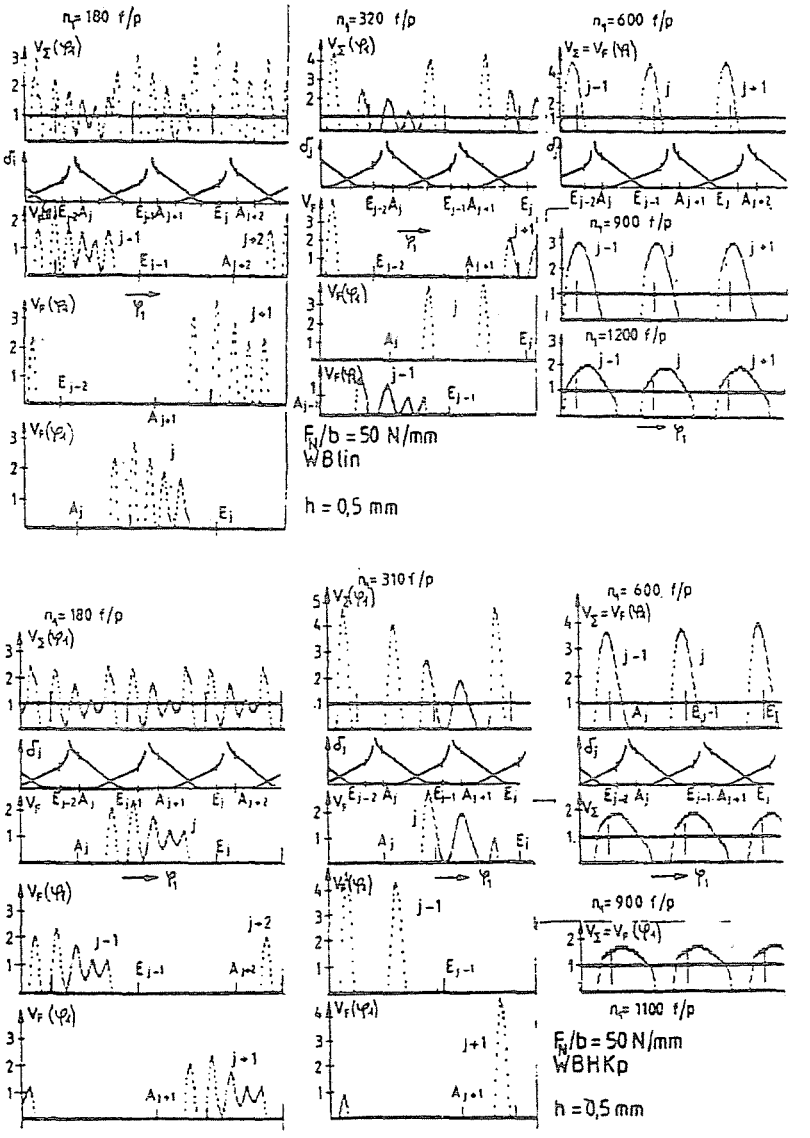

Fig. 12. Contact force and single tooth force dynamic factors at given constant input speeds, for two different single tooth pair stiffness values

the period of the excitation (being equal to the period of one pitch length) and limited tooth flank separation zones develop,

- at $n_1 = 320$/min, one can find a double period response vibration, with important tooth flank separation zones,
- at $n_1 = 600$/min, the period of the vibration equals the period of the excitation and there is only one tooth pair contact, around the pitch circle, so the length of angular intervals with zero force (tooth flank separation) are important,
- at $n_1 = 900, 1200$/min, the basic vibration shape remains similar, with increasing one tooth pair contact zones.

For the non-linear single tooth pair stiffness case, WBHKp, similar response vibrations are found, however, the contact force elevations are considerably reduced.

As it was seen on resonance curves of *Fig. 11* at low load level, the real unstable regions displace to smaller speeds and do not correspond of the theoretical $\widetilde{N}$ values. The reason of that is the development of the tooth flank separations on more or less long angular intervals, leading to the softening of the system, i.e. with 'contact intervals' without contact, so with zero stiffness.

Based on the contact force functions on *Fig. 12*, one can identify the real stiffness values of the system at each contact point, with zero stiffness on the zero load intervals. Determining the integral mean on one vibration period of the 'realised stiffness function', one can find a more softer system, as it should be without tooth flank separations, i.e. with tooth contact during the whole vibration.

Table 1 contains for the two stiffness cases at the given speeds, the 'real' gear engagement stiffness $\widetilde{c}'_\gamma$, and the input speeds $\widetilde{n}'_{1s}$, which introduces the excitation involving the main resonance, i.e. the resonance to $N = 1$.

Table 1. Tooth engagement spring stiffness values and input speeds to $N = 1$

	WBlin		WBHKp	
n_1 [1/min]	$\widetilde{c}'_\gamma$ [N/mm ·μmm]	$\widetilde{n}'_{1s}$ [1/min]	$\widetilde{n}'_{1s}$ [N/mm ·μmm]	$\widetilde{n}'_{1s}$ [1/min]
180	11.54	866	8.24	702
310	–	–	5.87	593
320	8.84	727	–	–
600	5.04727	549.4	–	–
900	8.84	727	4.19	500
1100	–	–	7.17	655
1200	11.7	837	–	–

Fig. 13 represents the excitation frequency values corresponding to the resonance at $N = 1$, expressed in input speed $\tilde{n}'_{1s}$, in the function of the input speed n_1. On the diagram, there are marked the different νth order resonances to different kth order Fourier components of the excitation function, which fall together, see chapter 2.2., *Eqs* (3), (4), (5). The thin line is the line, where $\tilde{n}'_{1s} = n_1$. The intersection of this latter with the curves indicates the input speeds, which are just the speeds, involving excitation frequencies to the main resonance, at $N = 1$. This permits us to identify approximately the resonance order of the different peak values on the resonance curves, i.e. which $\tilde{N}$ value can be attributed to them.

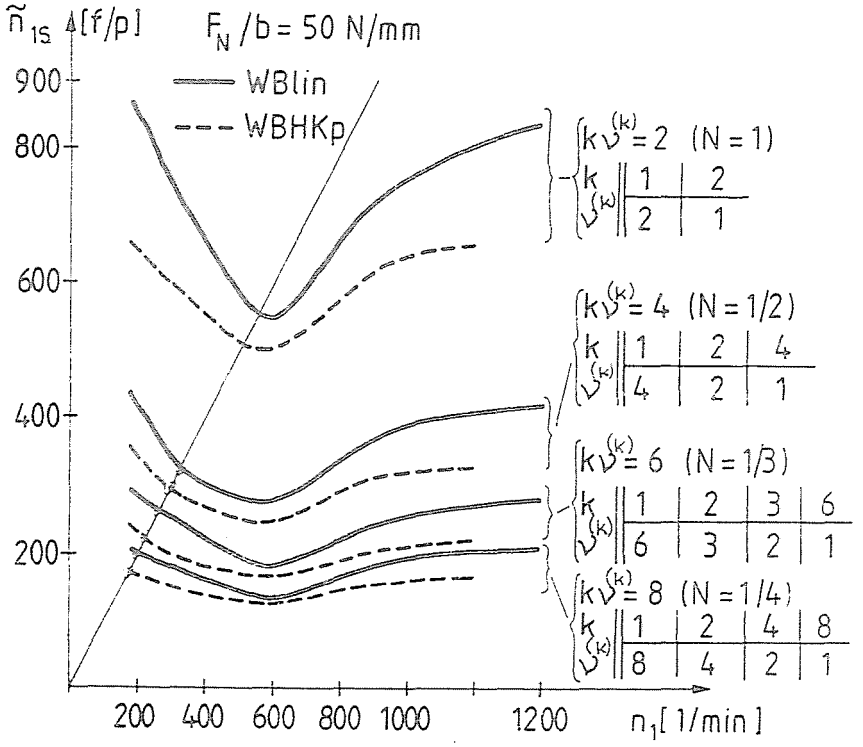

Fig. 13. Resonance frequencies expressed in pinion speed versus pinion speed

Based on *Fig. 13* and the resonance curves on *Fig. 11*, $F_N/b = 50$ N/mm, the following can be concluded, for the case WBlin:

- at input speed interval 180/min $< n_1 <$320/min the resonances corresponding to $\tilde{N} = 1/4, 1/3$ develop,
- on interval 320/min $< n_1 <$600/min the resonances at $\tilde{N} = 1/2, 1$ are overrun, but the two unstable regions do not separate,
- at speeds $n_1 >$600/min the system is in overcritical region, and the resonance at $n_1 = 1450$/min is the overcritical one, with $\nu^{(1)} = 1$.

Similar conclusion can be drawn for the case WBHKp.

6. Conclusions

The simulation results of gear trains with normal involute profiles and with toothing with tooth tip relief presented in this paper have shown that even in the case of ideal tooth geometry, but with considering real mesh, i.e. taken into consideration of mesh irregularities due to tooth deflections at the beginning and end points of contact, non-linear system behaviour itself, as a result of kinematic excitation. In the case of profiles with tip relief, strong load dependent behaviour was found, with important vibrations at low load levels and tooth flank separations on broad speed intervals. The analysis of the vibrations at low load levels has shown that resonance regions move to lower input speeds and more resonance regions fall together. The results have shown that the single tooth pair stiffness characteristics have important effect on vibration characteristics.

In case of complex gear train dynamic simulations, the real tooth geometry parameters and mesh conditions, as components of the kinematic excitation, and real single tooth pair spring stiffness characteristics are to apply, for arriving to more realistic system response results.

References

[1] MUNRO, R. G. – YILDRIM, N. – HALL, D. M.: Optimum Profile Relief and Transmission Error in Spur Gears. *Proceedings of the Inst. of Mechanical Engineers.* Univ. of Cambridge. IMechE 1990. pp. 35–42.

[2] NIEMANN, G. – WINTER, H.: Machine Elements. Bd. II. Springer Vlg. Berlin, Heidelberg, New-York. 1985. (In German).

[3] MÁRIALIGETI J. (1995): Computer Simulation Study of the Influence of Tooth Errors on Gear Dynamic Behaviour. *Periodica Polytechnica Ser. Transp. Eng.* Vol. 23., No. 1–2, pp. 89–105.

[4] MÁRIALIGETI J.: Non-linear Vibrations and Chaos in Gear Train. *2nd European Nonlinear Oscillation Conference,* Prague 1996. Vol. 1. pp. 277–280.

[5] KLOTTER, K.: Vibration Theory. Bd. 1. Springer Vlg. Berlin, Heidelberg, New-York 1980. (In German).

[6] Calculation of the Load Capacity of Gears. DIN 3990. (In German).

[7] WINTER, H. – PODLESNIK, B. (1983): Tooth Stiffness Characteristics of Gears. Part 2. *Antriebstechnik,* Vol. 22. No. 5. pp. 51–57. (In German).